Journal of Energy Storage 24 (2019) 100788

Contents lists available at ScienceDirect

Journal of Energy Storage

journal homepage: www.elsevier.com/locate/est

Deriaz pump-turbine for pumped hydro energy storage and micro applications

Alessandro Morabito*, Guilherme de Oliveira e Silva, Patrick Hendrick

Aero-Thermo-Mechanics Department, Université Libre de Bruxelles, Brussels, Belgium

ARTICLE INFO

Keywords:
Deriaz pump-turbine
Variable geometry pump-turbine design
Pumped hydro energy storage (PHES)
Turbine scaling
Computational Fluid Dynamic (CFD)

ABSTRACT

The growing importance of the efficiency and operational range of pumped hydro energy storage (PHES) installations, especially for variable load operations, calls for the use of more efficient turbomachinery designs. Deriaz turbomachines are promising candidates, since, among other advantages, they can operate as reversible pump-turbines with high hydraulic efficiency over a wide range of operational loads. Deriaz pump-turbines are largely absent from the literature and this paper gives an overview of their design, application and performance features. Particular attention is given to the hydraulic characteristics and design of a downsized model (6-21 kW) suitable for micro-scale PHES applications. This paper provides a practical and easily-built method to implement a micro Deriaz pump-turbine runner which gives a good outline for design at high yield (about 90%). The analysis is supported by extensive numerical simulations for different working conditions and validated by experimental data. The results confirm the superior characteristics of Deriaz pump-turbines and validate the design process, which is described here for the first time.

1. Introduction

Given the increasing use of renewable energy sources (RES), which are intrinsically intermittent, energy storage technology is expected to play a crucial role in dealing with the frequent time mismatch between energy production and energy consumption [1]. This is particularly important for micro-scale energy systems, which offer low inertia and which are expected to become ever more common with the increase in decentralized energy supply systems [2]. Given its still largely untapped potential in most areas of the world, micro hydropower (5-100 kW) provides a significant contribution to future energy needs. Moreover, micro hydropower is an efficient, renewable, non-polluting electrical energy source with a long lifespan at high efficiency [3]. It is available in abundance naturally in falls, canals and rivers as well as artificially by means of dams or basins. Site requirements can therefore vary considerably which respect to flow rate and available heads [4,5]. Water turbines can be designed and manufactured to suit the site-specific available hydropower energy [6].

Pumped hydro energy storage (PHES) mainly differs from a classic hydro power plant by dealing with refilling the upper reservoir and, depending on the topology and the size of the plant, by the greater importance of working at partial load. To cope with the requirements of PHES plants in terms of partial load and reversibility, more careful turbomachinery selection is required [7]. Although pumps and turbines are designed for a particular flow rate, in practice they operate across a wide range of flow rates taking into account seasonal fluctuations in flow levels [8]. Often the turbomachinery will temporarily work in off-design conditions during transient periods. During these conditions, the flow separates at the impeller tips, in the impeller and in the diffuser or volute. Re-circulation may occur at the inlet or at the impeller exit, where fluid might flow back from the diffuser or volute. These off-design conditions not only reduce installation efficiency, but can also strongly affect its working life. Under such conditions, cavitation can damage the impeller while excessive vibrations can reduce bearing life and reliability or even cause a resonant oscillation in the entire pump system [9]. Catastrophic failures are unusual, but off-design operation for long periods of time can seriously reduce installation working life.

Care must be taken when estimating the margin of excess capacity required by the system (i.e. supplied by the pump or required at the turbine). These margins are given by manufacturers as guidelines for the safe working range of their turbomachines. Too large margin normally causes the turbomachinery to operate far from off-design conditions but with low efficiency, reducing its reliability and working life. It is also economically important to determine whether low efficiency at nominal operating conditions (and corresponding operating costs) will balance out the losses avoided from a lack of excess capacity at unusual

* Corresponding author.
E-mail address: alessandro.morabito@ulb.ac.be (A. Morabito).

https://doi.org/10.1016/j.est.2019.100788
Received 10 April 2019; Received in revised form 22 May 2019; Accepted 24 May 2019

Nomenclature

a_0	guide vane opening, mm
c	absolute velocity, m/s
C_p	Pfleiderer's correction, –
d	streamline gap, m
D	diameter, m
E	specific hydraulic energy, J/kg
H	head, m
K	spouting velocity coefficient, –
n	Nikuradze index. –
N	rotational speed, m, m^3/s
N_s	specific speed, m, m^3/s
Q	flow rate, m^3/s
R	radius, m
T	torque, Nm
u	peripheral velocity, m/s
V	energy loss fraction, –
z	number of blades –
w	relative velocity, m/s
α	absolute velocity angle, deg
β	relative velocity angle, deg
η	efficiency, –
μ	dynamic viscosity, Pa s
ν	kinematic viscosity, m^2/s
ξ	incidence attack, deg
π	power number, –
ρ	density, kg/m^3
σ	Thoma's cavitation coefficient, –
τ	slip coefficient, –
φ	discharge number, –
ψ	correction coefficent, –
ω	angular speed, rad/s
Ψ	head number, –
Ω	blade pivot angle, deg

Subscripts

11	unit factor
1	inlet
2	outlet
a	ambient
h	hydraulic
l	loss
L	liquid
mech	mechanic
m	meridional direction
md	model
n	nominal
opt	optimum
pm	pump
P	power
pty	prototype
r	radial
ref	reference
st	static
u	circumferential direction
t	turbine
th	theoretic
v	vapour
vol	volumetric

occasions.

In some hydropower installations, it takes only a few seconds to open a high-powered hydraulic turbine to switch from a partial load to a full load. Moreover, most of the pump turbines are required to start in less than two minutes. Control and technical issues take precedence over other economic considerations. Standard Francis turbines work day after day at very low openings and consequently at low efficiency. The danger of disturbance from a very extensive distribution network makes immediate emergency power necessary. In order to remedy this, a turbine with a maximum efficiency at a low opening is needed, and not at approximately 80% of the full load as for a Francis turbine of average specific speed. Fig. 1 shows how a Kaplan turbine might be the answer to this problem. However, Kaplan turbines are not usable under high falls (80 to 200 m or more) due to mechanical and hydraulic restrictions. So it is in fact Francis turbines used under such conditions, even though they perform poorly at partial loads. There is a need to find a hydraulic turbine of lower specific speed which works efficiently at sharp partial load and higher available head than a Kaplan turbine. Logically then, it seems that the purely axial concept of the Kaplan turbine has to be abandoned and a combination of Francis blades with variable pitch blades might be the answer: at first ambiguously called *Francis à pas variable* (Francis at variable pitch), this was subsequently named the Deriaz turbine. The Deriaz pump-turbine[1] demonstrates high efficiency over a wide range of partial load conditions, thanks to its combined governor setting which uses adjustable runner blades and guide vanes. The advantage of a Deriaz pump-turbine is merely mechanical and therefore a robust solution for PHES applications in remote areas as well. The wide operational range operating at synchronous speed without additional electrical equipment results in less hazard of failure in regulating power in charging or generating phases.

In this paper, for the first time, a brief literature review is used to show how Deriaz turbomachine can fill the gap left between Francis and Kaplan reversible turbines working ranges. The promising performances of Deriaz turbomachines (often kept confidential by manufacturers) are analyzed and discussed for a micro-scale model. The dimension of the selected model is especially suitable for micro-scale PHES, investigated from the recent decentralized energy storage research community [11–13]. There is a lack of information regarding the technical feasibility and efficiency of these small installations for different loads. Interestingly, the performance of the designed Deriaz pump-turbine is described both in pumping and generating modes by means extended Computational Fluid Dynamic (CFD) simulations. The discretisation process is discussed as the numerical modeling of the turbulent fluid flow and the results are compared with experimental data available to the authors.

This paper starts by describing the state of the art regarding the largely unknown Deriaz pump-turbine (Section 2). This section is

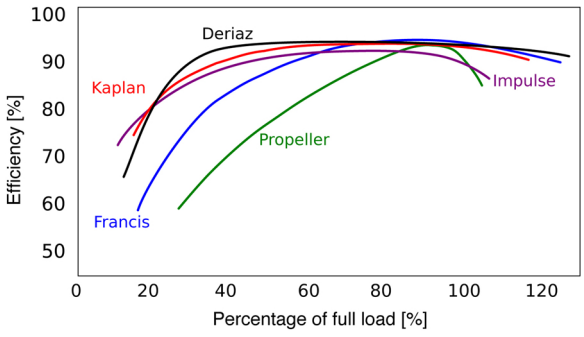

Fig. 1. Efficiency versus load of Deriaz turbine and most common turbines.

[1] or turbine-pump, as Deriaz hydraulic turbomachine has been devised as a turbine first [10].

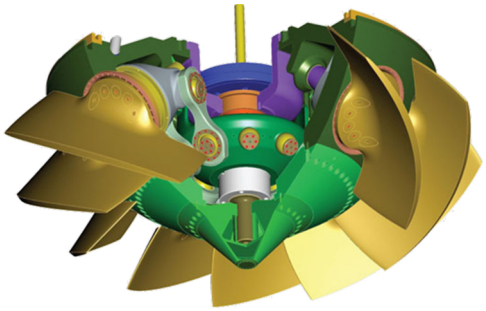

Fig. 2. Internal view of Deriaz pump-turbine runner and of its regulating mechanism in the hub [15].

needed to underline the features of this uncommon type of turbomachine. The Deriaz pump-turbine is a double regulated machine (guide vanes and runner blades) like Kaplan turbines but for medium-head plant. Therefore, the advantage of Deriaz turbines comparing to Francis turbines is the high efficiency operation over a wider range of head and discharge as well as an extended region with limited pressure pulsations. Section 3 examines the prototype and the downscaled model for micro PHES applications. In Section 4, the theory and design required to develop the used geometry is presented. Moreover, this section allows the readers to reproduce the results obtained. Flow behavior in CFD simulations is examined in Section 5, for part-load conditions at different operating points in turbine and pump mode. The results obtained match with the experimental data and confirm the versatile behavior of downsized Deriaz turbomachines as well as the validity of the model used.

2. Driaz adjustable runner blades regulation

The Deriaz hydraulic turbomachine, presented by engineer Paul Deriaz, was the first diagonal pump-turbine to be designed [14]. In contrast to most hydraulic machines, the flow in a Deriaz turbine does not follow a full axial or radial direction but is a diagonal mixture of the two. Deriaz turbines, like Kaplan turbines, have also adjustable blades. In fact, *Deriaz turbine is to the Francis turbine what the Kaplan turbine is to the fixed- blade propeller* [10]. The reduction of specific speed leads to a reduction in the radial extension at the leading edge of the runner and to a loss of axial alignment thereby giving a direction mix between axial and centripetal. From a mechanical point of view, to support the increasing hydraulic forces applied to the blades, their trunnions need to be larger and more resistant. The hydraulic conditions also require more blades with an increase in the ratio of blade length to spacing, which makes the placement of the large pivot bearings very difficult. This is because the increased energy difference between the inlet and outlet requires longer blades in order to avoid blade overloading.

The movable blade's length is limited at the root by the spherical geometry of the hub. Due to the limited space for the mechanism in the hub, the number of blades is also limited. The maximum number of blades is 10. This limits the maximum head for Kaplan turbines to approximately 60 m at reduced maximum efficiency.

The runner blade servomotor is normally a rotary type located inside the turbine shaft or runner hub. The rotation of the servomotor piston is transmitted to the spider inside the runner hub through the piston rod. Each connection of the spider and blade arm has a slide block which conveys the rotating motion of the spider to the runner blade stem (Fig. 2).

The Deriaz runner is characterized by the spherical surfaces of the hub and the skirt. This allows for the rotation of the blades whilst maintaining a narrow clearance and is an essential departure from the corresponding surfaces of the Francis toroid runner (Fig. 3).

For a machine at constant speed, the discharge diameter of the runner has a controlling effect on the total dynamic pumped head. The variation in mean diameters of the inlet and outlet edges of the blade resulting from blade movement is a remarkable operational advantage under variable head: closing the blades, for instance, the maximum diameter decreases, or rather, the radial extension ΔR decreases (Fig. 3c). The oblique position of the runner-blade pivots in the Deriaz pump-turbine gives the mixed-flow characteristics and the short radial extent of the vane-inlet edge [16].

The optimum feathering angle of the blades for higher heads is greater than for lower heads according to the accepted design of the flow speed field. The variation in mean diameters of the inlet and outlet edges of the blade has no equivalent in the purely axial Kaplan runner (Fig. 3b) locating the Deriaz machine between Francis and Kaplan turbines in terms of functionality where it also meets the need of all the frequent border cases between Francis and Kaplan turbines. The main difference in the blades from those of a traditional Kaplan turbine, is that their axes are not orthogonal to the turbine axis: the Deriaz offers runner shape adaptation based on the head available (Fig. 4). Corresponding to progressively higher heads the blade pivot angle Ω decreases, moving from a mainly axial configuration to a more radial one.

Another important design feature of the Deriaz pump turbine is that it is possible to create full contact between adjacent blades for the entire length of the edges to complete the closure (Fig. 5). Theoretically, the machine can therefore be shut down without using a conventional gate apparatus or inlet valve. The omission of the closing apparatus allows considerable simplification of the plant, leading to a smaller powerhouse and reduced costs.

Moreover, the versatile Deriaz turbine is designed to be used as a pump. The change of operation involves merely reversing the direction of rotation. It is only necessary to close the blade, shut down, (even with the head gate fully opened) and then restart [16].

Regarding a more global value such as efficiency, η, several tests comparing a Francis turbine of the same specific speed and size show how a Deriaz prototype can achieve a very flat curve and provides a better overall performance at partial load (Fig. 1). More recent studies have shown the improvement of a Francis solution for variable head reaching a comparable maximum value of efficiency, but still over a smaller load range than for a Deriaz machine [15]. Only Francis turbine units with variable speed compete to Deriaz pump-turbine in both operational modes.

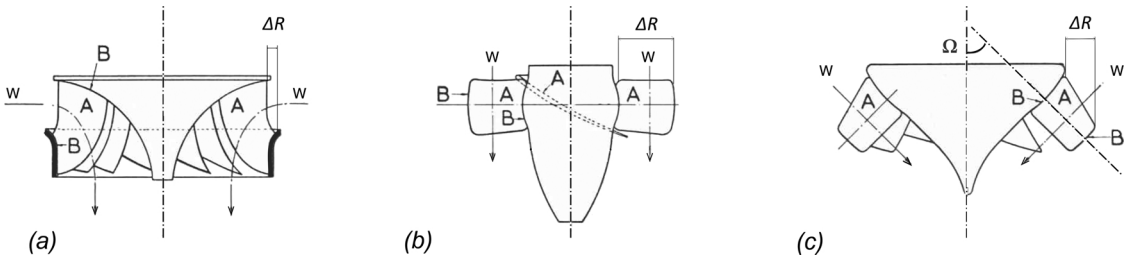

Fig. 3. (a) Francis runner; (b) Kaplan runner (c) Deriaz runner [10]. A: blades or adjustable blades; B: toroidal or spherical surface; W: direction of the flow; ΔR: radial extension of the runner blade.

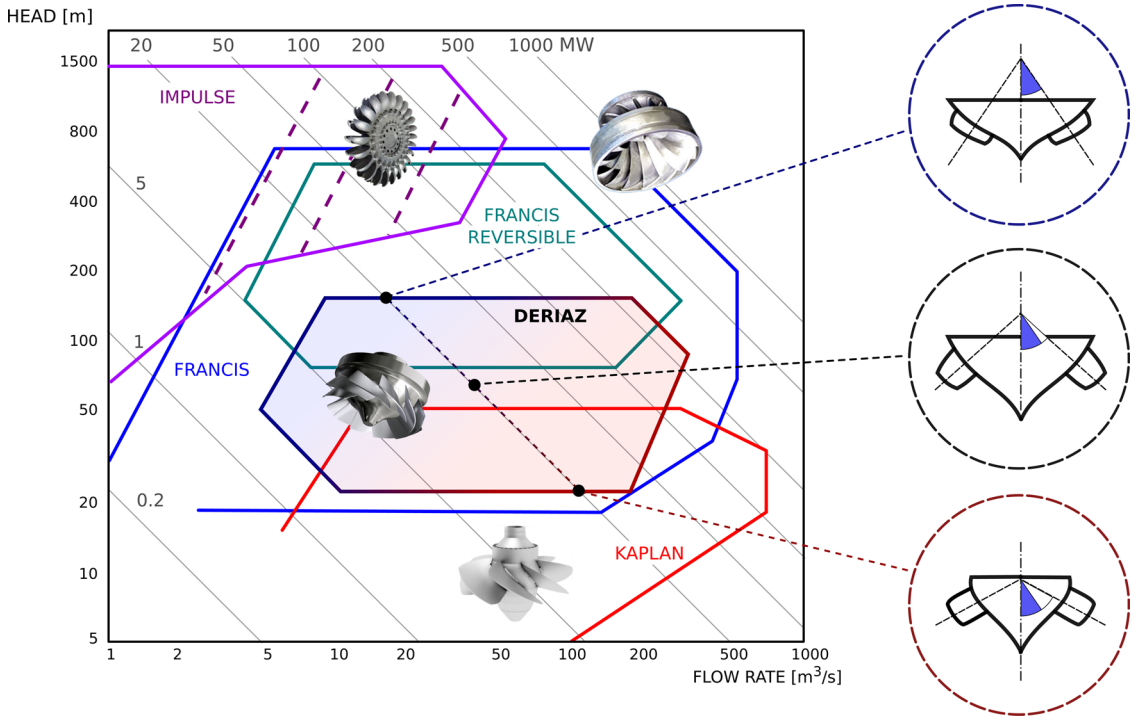

Fig. 4. Diagram flow rate over head for the most common hydraulic turbines and Deriaz turbine at different blade pivot angle Ω.

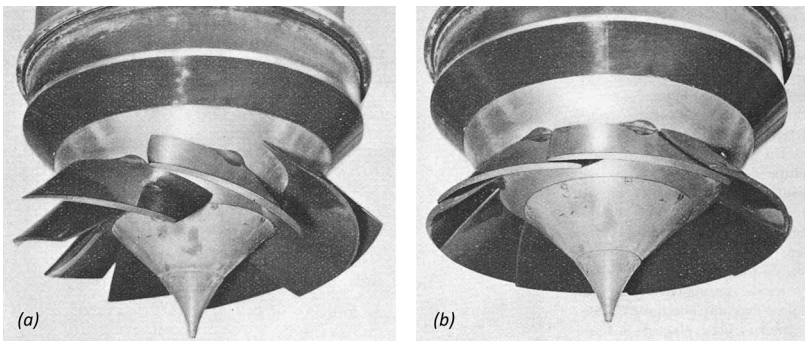

Fig. 5. Deriaz runner normally open (a) and closed (b) [10].

2.1. Pumped hydro energy storage

Pumped storage is currently by far the most common form of on-grid electricity storage. During off-peak hours, energy is stored in the upper reservoir by pumping water back. During peak hours, the water is released to the lower reservoir through hydraulic turbines which generate electrical power. The operational conditions of PHES are perfectly suited to a reversible turbomachine which can function as both a pump and a hydraulic turbine. A Deriaz turbomachine is able to do it by reversing its rotation direction. Moreover, they can adapt quickly to fluctuations in demands for electricity.

By using a reversible machine such as a Deriaz, a PHES plant can make better use of available space by reducing the size of the power house required. Available head might vary while the upper reservoir is refilling or emptying which will be more evident in small PHES systems where the volumes of water are usually smaller [7]. In addition, turbomachines can also work under variable rotation speeds. Some PHES systems couple the motor/generator to a frequency changer enabling a wider range of pumping or generating speeds [7]. The geometry of a Deriaz machine can also change by means of its adjustable runner blades thanks a to mechanical and or hydraulic system inside the rotor. It is thus possible to combine a high level of adaptability and efficiency in the same runner. This type of pump-turbine is extremely rare and it is installed around the world mostly around the 1960s. In fact, Francis turbines were usually preferred against the complex systems associated to the double regulation and high maintenance costs of Deriaz pump-turbine. However, today energy markets are changing and resulting in the need for more load following and frequency control operation of hydro assets [17]. In this context, the flexible storage alternative is becoming more and more a cost-effective option [18]. Table 1 provides a list of sites where Deriaz pump-turbine has been installed. In the following subsections, brief overviews of some site adopting Deriaz pump-turbine are presented in order to show further detailed features of the turbomachine.

2.1.1. Sir Adam Beck generating station – Canada

The 174 MW Sir Adam Beck Pump Generating Station and its 300-ha reservoir were constructed at the same time as the Sir Adam Beck II Generating Station [19]. Water diverted to the Sir Adam Beck generating complex is typically pumped into the reservoir at night so it can be used to generate electricity during subsequent periods of high demand. Six mixed-flow variable-pitch Deriaz pump-turbines are installed at the pump generating station and can fill the reservoir in about eight hours. The pumped-storage scheme enables a more effective use of the water that is available for power production under the Niagara Diversion Treaty of 1950 [19]. It offers a method for translating what would

Table 1
Pumped storage plants using Deriaz pump-turbine.

Power station	Size [MW]	Year	Country[a]	Nr unit
[19] Adam Beck	29	1954	CA	6
[23] Gangnan	11	1968	CN	1
[23] Miyun	22	1975	CN	2
Sesquile	100	1964	CO	2
[24] Valdecanas	75	1964	ES	3
[25] Nassauc	3	1995	FR	1
[20] Culligran	17	1966	GB	1
[26] Kadana	61	1977	IN	4
[27] Maharashatra	52	2012	IN	2
Ananaigawa	13	1964	JP	1
Kagedaira	46	1968	JP	1
[22] Kuromata II	18	1963	JP	1
Masegawa I	144	1976	JP	2
[28] Niikappu	100	1973	JP	2
[28] Takami	103	1983	JP	2
Takane I	88	1969	JP	4
[29] Niedzica	92	1997	PL	2
[30] Czorstyn	42	1990	PL	2
[31] Liptovsk	97	1975	SK	2
[32] Dos Amigos	18	1963	US	3

[a] Country code adopted by the two-letter Standard ISO 3166-1.

be surplus energy at times of low demand into primary energy at times of high demand. The change over from turbine to pumping sequence is accomplished in a matter of minutes and occurs several times each day. The guide vanes are equipped with adjustable flaps, which control the flow angle at the inlet of the turbine runner and are deflected according to the head level Fig. 6. When the machine works as a pump these vanes function as a diffuser and the flaps are placed in line with the vanes so as to not increase hydraulic losses.

2.1.2. Culligran plant – Great Britain

The Culligran site is located in a Scottish National Reserve where a 17 MW, 10 blades Deriaz turbine is coupled with a 2 MW Francis turbine [20]. Scottish and Southern Energy plc invested in an 18-month project to refurbish the 43 years old, Deriaz turbine in order to extend the plant's operating life by a predicted further 30 years' without further major refurbishment or significant capital expenditure and to maximize efficiency and output. The runner chamber of the turbine was suffering from severe cavitation and it took 12 manufacturing facilities throughout Europe to manufacturer all the components [21]. Particularly high machining precision was needed to not exceed the 1.5 mm gap between the blades and the chamber wall so as to avoid cavitation or the disastrous consequences of blades coming into contact with the chamber wall. Modern computational tools (CAD, CFD and FEA) were used in the design and testing of the new Deriaz runner to ensure that the requirements of the project were met [21].

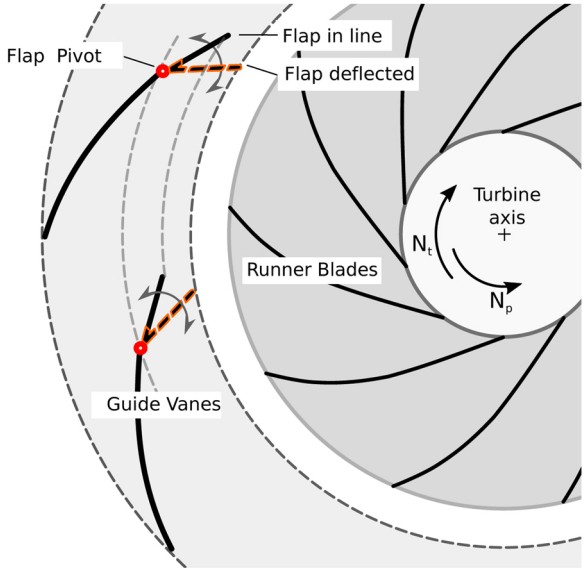

Fig. 6. Radial view of Deriaz turbine guide vanes installed in Sir Adam Beck Station.

2.1.3. Kuromatagawa plant – Japan

Kuromatagawa II power station adopted a vertical shaft Deriaz pump-turbine in 1963 in order to deal with a large head variation and to attain high efficiency at partial load. The maximum available head in this case is twice the minimum operational head (39 m) [22]. Moreover, the pump-turbine, coupled with a pole change generator-motor, have two speed operations in order to improve performance. The ratio of unit speeds at maximum efficiency during turbine and pump operation is about 1.1, the same as for the Francis type pump-turbine [22]. In Kuromatagawa plant, the Deriaz operates at 333 rpm during pumping at high head and 300 rpm in turbine mode from an effective head of 78 m to 39 m with a maximum discharge of 28 m^3/s [22].

3. Deriaz hydraulic modeling

In the presented article, a micro-scale model Deriaz pump-turbine (md) is designed based on the runner geometry of an existing prototype case (pty) and all the profiles necessary to describe the runner blade are calculated. The design aims to provide an outline of a Deriaz pump turbine for micro application. The hydrodynamic and mechanical solutions are designed taking into account that the efficiency is not a priority criterion for the micro hydropower units but relatively high performance in a wide range of partial load.

3.1. Prototype Deriaz pump-turbine in Naussac

The prototype is installed in the power/pumping station of the Naussac II (Fig. 7). This is the second phase of the Naussac I reservoir development which is used to maintain the low-water flow in the Allier river as well as in the Loire river downstream of its confluence with the Allier. Specifically, the plant of Naussac II is intended for the support of low-water mark of Allier and the Loire; the functioning of machines was thus optimized in pump to favour the filling of the reservoir, and not the hydroelectric production which is a by-product.

This installation was preferred over a double or multi-speed Francis machine which would have required a much larger pumping basin [25]. This would have required intake works on the dam of more than 10 m height in contrast to only 2.30 m with Deriaz machines [25] – a much better scenario ecologically and for its reduced impact on the

Fig. 7. View of Naussac II power-house.

Table 2
Mechanical data of Deriaz prototype working in Naussac II.

Turbine Specifications		
Rotational speed, N	750	[rpm]
Diameter of the entry of the spiral case	1.140	[m]
Number of fixed stay vanes	12	[–]
Number of mobile wicket gates	24	[–]
Height of the distributor at runner entrance	0.257	[m]
Distributor boring diameter	1.286	[m]
Runner diameter, D	0.950	[m]
Number of runner blades, z	8	[–]
Blade pivot angle, Ω	45	[deg]
Width of the draft tube outlet	2.592	[m]
Height of the draft tube outlet	1.130	[m]

landscape. In addition, polluting fluids such as oil from the moving parts of the machine in contact with the water have also been partially eliminated [25], addressing water quality concerns. The hydrostatic seal-joint and the controls of the blades of the runner have a waterproof ceramic coating, as do the gates downstream.

The existing installation was commissioned in 1983, creating a reservoir with a capacity of 190 Mm^3. The power station has three identical Deriaz pump-turbines of 0.950 m in diameter with a unitary power of 3 MW during pumping, each able to generate a maximum of 2.6 MW. Each group is coupled to an asynchronous classic motor-generator, all fed by a single transformer of 12 MVA. The synergy of the blade and guide vanes regulations allows the groups to function well under the variable working conditions. The unit pumping flow is variable from 2 to 5.5 m^3/s under a head varying from 32 to 57 m. The Naussac II plant is primarily intended to support the low-water mark of Allier and the Loire rivers [25]. So, the machines were optimized to fill the reservoir by pumping rather than for hydroelectric production.

The speed of every group is regulated by inductive sensors and the rotation direction is detected by two specific sensors. During the startup phase, the regulator maintains the machine close to the synchronous nominal speed, allowing it to be coupled to the network. Once the group is coupled with the network, the regulator maintains the optimal water flow rate for pumping or generating. During normal functioning, the machine is relatively noisy until a flow rate of about 3.5 m^3/s after which it becomes quiet. As highlighted during the model testing for this prototype in Naussac II, the cause of the noise is cavitation. This is considered completely acceptable if the wheel blades are made of a stainless material to limit excessive damage.

The regulator has two conjugate cams, one for the functioning of the pump, the other one for the functioning of the turbine. This ensures the best combination of blades and vanes giving the best possible efficiency overall the variable conditions for pumping or generating.

The prototype is moderately sized, adapted to the maximum flow value of the project. The main mechanical characteristics are shown in Tables 2 and 3.

3.2. Selected model case

The hydraulic study of these diagonal reversible turbines with double a regulation type Deriaz was conducted on a reduced scale model with a reference diameter of 0.3 m. Experimental performance analysis on this model size has been conducted and reported by [34–36]. The small size of these machines makes manufacturing them more complex; the construction of the operating mechanism for eight blades tends to be more difficult in a smaller space than for a bigger prototype or for a Kaplan turbine. For these reasons, a diagonal flow turbine has a compact arrangement for the runner blade operating mechanism, as shown in Fig. 2.

In the scale model only the hydraulic internal passage design has been converted, using the diameter ratio between prototype and model D_{pty}/D_{md}, as the geometric scale ratio. Geometrical similarity in both

Table 3
Operational data in pumping and generating Deriaz prototype in Naussac II power-plant [25,33].

Pump mode		
Geometrical reference, D	0.950	[m]
Rotation speed, N	750	[rpm]
Nominal power used per unit, P_p	3	[MW]
Corresponding flow per unit Q_p	4.6–5.5	[m^3/s]
For a total vertical height, H_p	48.7–58.2	[m]
Total losses for max height	1.2	[m]
Number of units in service	3	[–]
Efficiency, $\eta_{t,h}$	85.5	[%]
Turbine mode		
Geometrical reference, D	0.950	[m]
Rotation speed, N	750	[rpm]
Maximum power per unit, P_t	2.65	[MW]
Corresponding flow per unit, Q_t	5.4–6.0	[m^3/s]
For a net head height, H_t	50–57	[m]
Total losses at max height	0.5	[m]
Efficiency, $\eta_{t,h}$	92.8	[%]

downsized and full-size turbomachines may be attained without great difficulty. In general, it is more difficult to attain similarity in relative roughness and for the clearances between the runner and stationary elements, both from a technological and a hydrodynamic point of view. The discussion on the performances on the designed Deriaz model is based on affinity geometric laws scaled on the two machines.

The Reynolds' law of similarity assumes that friction losses are the same in both machines. However, this assumption is not valid everywhere. In fact, the friction is a function of the surface roughness and Reynolds number, *Re*. Therefore, defining water as the working fluid at comparable temperatures, the same viscosity is assumed for the model and the full-size prototype although adjustments must be taken into account as depicted in the following sections.

The performance of the model is also more efficient, mostly due to the simpler hydraulic system and components [34]. The study described in this paper starts by analysing the machine in several cases in turbine and pump mode. After simulating the machine over a wide range of conditions several characteristic curves can be compiled in order to choose the main mechanical parameters for the model design.

3.3. Scaling laws

Fluid mechanics and turbomachine performance are severely influenced by scaling laws. The affinity laws analysis is applied to the Deriaz prototype and Deriaz model in order to predict the performance of the turbomachine operating at different speeds and flow rates. Hardly the geometrical and kinematic similitude are achieved for a viscous fluid as water. In fact, on the turbomachine scaling it is not possible to use directly the Reynold's similitude

$$\mathrm{Re} = \left.\frac{\rho U_{\mathrm{ref}} L_{\mathrm{ref}}}{\mu}\right|_{\mathrm{pty}} = \left.\frac{\rho U_{\mathrm{ref}} L_{\mathrm{ref}}}{\mu}\right|_{\mathrm{md}} \quad (1)$$

where U_{ref} and L_{ref} are the flow speed in m/s and length in m adopted as reference [37]; the subscripts "pty" and "md" represent respectively prototype and model. In this analysis the velocity $U_{ref} = \omega D$ and the L_{ref} is mean flow diameter, D. Fig. 8 illustrates a Deriaz turbine scaled model used for the design of the new runner installed in Culligran [21].

If the model testing is done using the same working fluid ($\nu_{md} = \nu_{pty}$) and the geometrical scale range is quite large, it is difficult to maintain a suitable velocity. As consequence, it is necessary to predict the possible variation of the velocity field and losses, due to dissimilar Reynolds number, Re (Eq. (1)).

Re is greater in the prototype than in the downsized model. Hydraulic losses have to be reviewed and the efficiency, η_h, has to be corrected as well. Since the hypothesis to consider the flow as completely turbulent remains valid, it is possible to use the Stodola-

Fig. 8. Downsized model of a Deriaz pump-turbine [21].

Ackeret's rule [38] for the scaling of efficiency

$$\frac{1-\eta_{\text{pty}}}{1-\eta_{\text{md}}} = (1-V) + V\left(\frac{\text{Re}_{\text{md}}}{\text{Re}_{\text{pty}}}\right)^{n} \tag{2}$$

The first term of the equation represents the ratio of the losses prototype/model in two homologous functioning points. V represents the loss part due to the Re effect on the model and so $(1-V)$ is its complementary. The value V comes from the experience of the designer and from previous experiments: as the amount of previous statistical results is practically zero, the value assumed here is 0.5. n is an index offered by Nikuradse experiences [39] for localize the kind of fluid dynamic losses, here assumed at 0.2. The terms V and n are different according the literature depending by the accuracy of their data and dependency by the Reynolds number [38,40,41].

The analogy for two turbomachine is referred to the corresponding Best Efficiency Point (BEP). Eq. (2) offers the estimation:

$$\Delta\eta_{\text{opt}} = \eta_{\text{pty,opt}} - \eta_{\text{md,opt}} \tag{3}$$

3.4. Application of the scaling in pump mode

The discussion of the efficiency in pump mode on the scale model is based on to the ratios D_{pty}/D_{md} and N_{pty}/N_{md}, where the fixed rotational speed of the model, N_{md}, is set to 1054 rpm. Other complementary information are listed in Table 3. The assumption that the two machines are using the same fluid at comparable temperature and kinematic viscosity, ν, is maintained. From the definition of Reynolds number Eq. (1)

$$\left(\frac{\text{Re}_{\text{md}}}{\text{Re}_{\text{pty}}}\right)_{\text{opt}} = \frac{N_{\text{md}}D_{\text{md}}^2}{N_{\text{pty}}D_{\text{pty}}^2} = 0.140 \tag{4}$$

Finally, using Eq. (2)

$$\frac{1-\eta_{\text{pty,opt}}}{1-\eta_{\text{md,opt}}} = 0.837 \tag{5}$$

With $\eta_{md,opt} = 0.855$ (Table 3), the difference in the efficiency between the two machines in pump mode, $\Delta\eta_{h,pm}$, results

$$\Delta\eta_{h,\text{pm}} = \eta_{\text{pty,opt}} - \eta_{\text{md,opt}} = 2.81\% \tag{6}$$

3.5. Application of scaling in turbine mode

As is previously calculated for pump mode in Eq. (6), an efficiency correction must be conducted for turbine mode as well. Using Eq. (2) and the value reported for $\eta_{pty,opt} = 0.928$ in Table 3, the difference in the efficiency between the two machines in turbine mode, $\Delta\eta_{h,t}$, result in

$$\Delta\eta_{t} = \eta_{\text{pty,opt}} - \eta_{\text{md,opt}} = 1.40\% \tag{7}$$

The coefficients, n and V, in turbine mode are taken equal to the pump mode, because larger variation in velocity field are not expected.[2]

3.6. Additional scaling considerations

The transposition is in agreement with the methodology provided by IEC code no. 60193 [37]. In this case, a reference Reynolds number of $7\cdot10^6$ is considered to minimize the deviation

$$(\Delta\eta_h)_{\text{pty}\to\text{md}} = \delta_{\text{ref}}\left[\left(\frac{\text{Re}_{\text{ref}}}{\text{Re}_{\text{pty}}}\right)^{0.16} - \left(\frac{\text{Re}_{\text{ref}}}{\text{Re}_{\text{md}}}\right)^{0.16}\right] \tag{8}$$

where $\delta_{\text{ref}} = (1-\eta_{h,\text{pty,opt}})/\left[\left(\frac{\text{Re}_{\text{ref}}}{\text{Re}_{\text{pty,opt}}}\right)^{0.16} + \frac{1-V_{\text{ref}}}{V_{\text{ref}}}\right]$ with V_{ref} equal to 0.8 for operation as turbine and 0.6 for operation as pump. The values of $\Delta\eta_{h,pty\to md}$ divergences with the results of Eqs. (6 and 7) by less than 0.2%.

The efficiency variation presented in Section 3.3 is with respect to only the hydraulic aspects, η_h, and other considerations must be undertaken. In the reduced geometry, the inner domain of the machine is simpler than the prototype. For instance, a classic hydraulic machine for power production is equipped with internal access doors for maintenance and inspections. These can cause leaks and important efficiency losses. Moreover the hydraulic turbomachine is usually connected to the whole gear apparatus and to the auxiliaries which produce additional load effects. All the subsequent discrepancies are summarized in variations of further hydraulic losses, leaks and mechanic losses:

$$\Delta\eta = \Delta\eta_h - \Delta\eta_{\text{vol}} - \Delta\eta_{\text{mech}} \tag{9}$$

Consider a same class of turbomachines that work under similar conditions. For these turbomachines a series of dimensionless coefficients are equal

$$\Psi = \frac{\text{gH}}{U_2^2} \quad \varphi = \frac{Q}{U_2R_2^2} \quad \pi = \frac{P_p}{\rho U_2^3R_2^2} \tag{10}$$

where Ψ is called the dimensionless *Head coefficient*, φ is the dimensionless *Flow rate coefficient* and π is the dimensionless *Power coefficient*. Note that the mechanical losses and the total efficiency of a pump do not follow the similarity rules. The power coefficient is defined only for the internal power. For a constant value of the specific speed, N_s, the two machines belong in the same class. In order to treat each parameter individually, it is necessary to re-write the equation with $\Psi = \frac{\text{gH}}{U_2^2} =$ constant, which means $H \propto (D_n)^2$. Finally, it is possible to compute the term as

$$\frac{N_{\text{md}}Q_{\text{md}}^{1/2}}{\text{gH}_{\text{md}}^{3/4}} = \frac{N_{\text{pty}}Q_{\text{pty}}^{1/2}}{\text{gH}_{\text{pty}}^{3/4}} \Rightarrow$$
$$\Rightarrow \frac{NQ^{1/2}}{\text{gH}^{3/4}} \propto \frac{(ND)^{3/2}}{H^{3/4}} \propto \frac{ND}{H^{3/4}}H^{1/4} \propto \frac{ND}{\sqrt{H}} \tag{11}$$

Thus, the net head in pump mode of the model, $H_{p,md}$, respects the similitude

$$H_{\text{pty}} = H_{\text{md}}\frac{N_{\text{pty}}^2D_{\text{pty}}^2}{N_{\text{md}}^2D_{\text{md}}^2} = H_{\text{md}}\cdot 5.07 \tag{12}$$

Indeed, for $H_{md} = 10$ m, H_{pty} is equal to 50.7 m and it fits in the prototype head range according to Table 3. Likewise, the flow rate Q_{md} can be calculated according to

[2] This value is indicative. It is necessary to adduce further researches for determining more calibrated n and V in pumping and generating mode.

Table 4
Mechanical data of Deriaz prototype working in Naussac II.

Downsized model		
Geometrical reference, D	0.3	[m]
Design pumping head, $H_{p,n}$	10	[m]
Rotation speed, N	1054	[rpm]
Design pumping flow rate, $Q_{p,n}$	0.24	[m^3/s]
Pump efficiency, $\eta_{p,h}$	82.7	[%]
Turbine efficiency, $\eta_{t,h}$	91.4	[%]

$$Q_{\text{pty}} = Q_{\text{md}} \frac{N_{\text{pty}}}{N_{\text{md}}} \left(\frac{D_{\text{pty}}}{D_{\text{md}}} \right)^3 = Q_{\text{md}} \cdot 22.59 \tag{13}$$

and with the prototype maximum flow rate $Q_{pty} = 5.50\ m^3/s$ (Table 3), Q_{md} is equal to $0.24\ m^3/s$. Table 4 summarizes the operational data of the scale model.

4. Hydraulic design of the pump

The predictable pressure distribution inside the pump shows the fluid passes the impeller via an adverse pressure gradient. This further complicates the design of a turbine in pumping mode for all pump-turbines. The purpose of this research is to develop a procedure for preliminary steps of its design. The flow through the hydraulic turbine of the Deriaz type is quite complicated – as in most pump-turbines – and can require high demand on computer memory and CPU time [42]. Moreover the hydrodynamic design of a new impeller using inverse method is usually based on a already existing base design [43–45]. This section proposes a fast set of guidelines for designing mix-flow Deriaz pumps: the design methodology is classical one but has no precedent in Deriaz application in the literature.

4.1. Impeller inlet

The blade is shaped using a point by point method which defines the geometric parameters along five streamlines from the leading edge of the blade up to its trailing edge. The estimation of the field of the velocities for the whole of the leading edge of the pump blade starts with the calculation of the flow and principal streamlines along the midstream.

Euler's equation [46] is deduced on the assumption that the flow though the impeller is axi-symmetric and the velocity field is created by an infinite number of contiguous stream surfaces and an infinite number of blades of thickness equal to zero. In reality, the impeller has z number of blades of thickness which both reduce the cross-section area available for the flow through the impeller.

Blade thickness is a mechanical design consideration and dependent on the production technology used. It has to be thin enough to save material and weight, but also thick enough to handle fluctuating load flows and avoid the risk of fatigue cracks. The effective flow rate is also affected by the volumetric efficiency; the volumetric and mechanical efficiency are assumed to be 98% for an open impeller pump [39,47,48]. The velocity in the impeller inlet and outlet in the meridional direction c_m is given by [47]

$$c_{m1} = K_1 \sqrt{2gH}, \quad c_{m2} = K_2 \sqrt{2gH} \tag{14}$$

where K_{cm1} and K_{cm2} are respective velocity non dimensional coefficients [47,48] which summarize the divergence from the theoretical value of the Bernoulli velocity.

The inlet flow direction is not normally considered completely axial and the peripheral component of the absolute velocity c_u is not equal to zero for most of the inlet edge of the blade. The theoretical head H_{th} is consequently affected by Euler's equation and this phenomenon is more pronounced at low partial loads. Pre-rotation and reverse flow result in an abnormal variation in pressure at the suction pipe wall and the rise in noise and vibration results in mechanical damage. In order to control these phenomena, IGVs (Inlet Guide Vanes) can be placed a short distance from the impeller inlet. Variable angle adjustment of the IGVs can help regulate the head and increase efficiency over a fairly wide range of mass flow rates. However, IGVs need supplementary components and produce a pressure loss and a variation of the cavitation critical point [49].

In order to attain the required discharge, it is necessary to increase the blade angle β_1 calculate from Eq. (15) by the angle of incidence ξ. Larger ξ values are used for bigger D_2/D_1 ratios and for larger calculated β_1 angles (as in short blade impellers) [47]

$$\beta_{1,\text{th}} = \arctan \frac{c_{1m}}{u_{1m}}, \quad \beta_1 = \beta_{1,\text{th}} + \xi_1 \tag{15}$$

If the approach flow angle drops below the blade angle ($\xi > 0$), the stagnation point is situated on the pressure surface of the blade. If the pump flow rate exceeds the shockless entry value, the incidence is negative and the stagnation point is located on the blade suction surface [39]. Values of ξ are in the range [2°, 6°] and the angle β_1 usually lies between 15° and 30° although in some cases it may be as high as 45° [47,39].

4.2. Impeller outlet

The theoretical head pump equation is defined as the head that a pump could generate if there were no hydraulic loss or mechanical friction during the operation of the pump. Combining this with and the velocity triangle at the outlet we obtain

$$u_2 = \frac{c_{m2}}{\tan \beta_2} + \sqrt{\left(\frac{c_{m2}}{2 \tan \beta_2} \right)^2 + gH_{\text{th}} + u_1 c_{u1}} \tag{16}$$

The hydraulic resistances in the passages and the disk friction of the shroud rotating in the liquid absorb a considerable part of the power of the machine and lower its efficiency. In the first model iteration, the velocity at the outlet, c_{m2}, is taken as being somewhat less than the velocity at the inlet according to the values for K_1 and K_2, within the range $c_{m2} = [0.7, 0.75]c_{m1}$ [47].

Since the velocity pattern in a turbomachine results from the pressure field around the blades, it can be concluded that different flow conditions are present on the pressure and suction sides of the blade. Hence the flow is not able to follow the blades exactly. The condition of flow *blade-congruent* is theoretically reachable with an infinite number of blades [39]. The difference between the theoretical and absolute fluid tangential velocities is described by the following equation: slip $= c_{u2} - c_{u,\infty}$. Several values for the slip factor have been cited in the literature [40,50].

The components of the rotor exit velocity diagram are shown in Fig. 9, which depicts the relationship between the absolute and relative velocities and flow angles.

The actual head rise is calculated iteratively in terms of the inlet and exit velocity triangles and the rotor hydraulic effectiveness, ε_{hyd}, which is the ratio of theoretical head to the theoretical head with infinite blades

$$\varepsilon_{\text{hyd}} = \frac{H_{\text{th}}}{H_{\text{th},\infty}} = \frac{1}{1 + C_p} \tag{17}$$

Pfleidere's correction, C_p, for a finite number of blades is calculated from the semi-empirical formula [40]

$$C_p = \psi \frac{r_2^2}{z T_{\text{st}}} \tag{18}$$

where r_2 denotes the external radius of the impeller with z blades, T_{st} the static moment of the midflow streamline with respect to the axis of

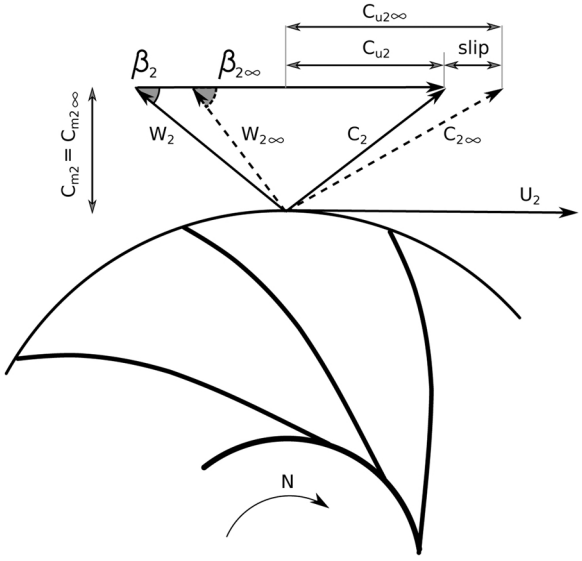

Fig. 9. Slip factor effect on velocity triangle. Slip is defined as $\Delta c_u = c_{u2} - c_{u,\infty}$.

rotation and the value of the coefficient ψ depends on the type of the impeller.[3] For impellers curved in three dimensions [47]

$$\psi = [1.0\ 1.2](1 + \sin\beta_2)\left(\frac{r_1}{r_2}\right) \tag{19}$$

As shown by Fig. 9, the vectorial tangential components of the fluid velocities are

$$c_{u2} = c_2 \cos\alpha_2 = u_2 + w_{u2} \tag{20}$$

$$w_{u2} = c_{m2}\tan\beta_{th,2} + u_2(1 - \tau) \tag{21}$$

The slip factor, τ, is defined as

$$\tau = 1 - \frac{\text{slip}}{u_2} \tag{22}$$

The deviation is the difference between the relative angle and the blade angle at the rotor exit as described by the following equation

$$\xi_2 = \beta_2 - \beta_{th,2} \tag{23}$$

Values for the slip coefficient have been reported in the literature starting with Busemann in 1927 and later with several reviews [50,51]

$$\tau = 1 - \frac{(\sin\beta_{th,2})^{0.5}}{z^{0.7}} \tag{24}$$

or slip values as Pfleiderer's [40]:

$$\text{slip}_{\text{Pfleiderer}} = \frac{g}{u_2}\frac{C_p}{1 + C_p}H_{th} \tag{25}$$

or Stodola's:

$$\text{slip}_{\text{Stodola}} = \frac{\pi \sin\beta_{th,2} u_2}{z} \tag{26}$$

The relationship Eq. (25) will be used in subsequent procedure for determine the slip coefficient. It is important to clarify that the slip does not represent a loss. It only affects magnitude of the head that the designed impeller can provide increasing the blade angle β_2.

In the case of study, the runner blades range has been chosen between 0° to +15° with the designed shape of the blade assigned at $\delta\beta = +10°$. Moreover the guide vanes opening is defined geometrically by the free distant a_0 offered by two couple of blades: from 0 mm to a maximum of 36 mm.

[3] It has been confirmed experimentally that for angles $\beta < 90°$ the number of the blades has negligible influence on the value of ψ. However, the influence of Reynolds number on ψ has not been satisfactorily explained. Conversely, with radial blades (having inlet and outlet angles of 90°) the slip factor is primarily caused by the Coriolis force.

Table 5
Design values along five main streamlines.

Streamline	d_I [m]	β_1 [°]	$1+C_p$	β_2 [°]	τ_{Pfl}/τ_{Sto}	w [m/s]
INT	–	19.12	1.323	9.63	1.0129	16.75
AA	0.0342	17.80	1.404	8.78	1.0128	18.34
BB	0.0324	16.78	1.490	8.13	1.0137	19.81
CC	0.0311	15.98	1.571	7.64	1.0140	21.07
EXT	0.0301	15.32	1.689	7.08	1.0183	22.71

In order to calculate angles β_1 and β_2 and hence to determinate the shape of the blade, the impeller is divided in five elementary streams of equal rate flow. Assumed the component velocity, c_m, maintains a constant mean value along each section [47] and that is used incompressible fluid, the streamlines are determined by trajectories which are able to divide the blade in section with the same total flow size.

The results are divided by five different streamlines along the runner blade, starting from the line close to the shroud (INT) to the one at the root of the blade (EXT). The distance from the next streamline is represented by variable d that divide the blades in section tread by same amount of flow rate (Table 5). The higher value obtained for C_p at the tip of the blade underlines the discontinuity of the available head at the trailing edge. This has not to be considered as a loss but hydraulic consequence of having finite number of blades as described by effectiveness (Eq. (17)). The ratio of the two different slip factor provides a certain level of confidence of the results obtained concerning the estimation of the slip factor: the values of τ for Stodola (Eq. (26)) and for Pfleiderer (Eq. (25)) in agreement.

4.3. Blade profile

Deriaz machine runner blades are no more complex in shape than those of a Kaplan, but they have an important design feature already mentioned: adjacent blades can be made to come into contact with each other over their entire width in the closed position (Fig. 5). This is an essential difference from the Kaplan where, in a closed position, the blades may be in contact at the periphery while a large gap remains between the blades near the hub [16].

Basically, in the short passage the angle of divergence may suddenly increase to suddenly resulting in flow separation and relative losses; in the long passage the flow comes into contact with more surface, thereby increasing friction losses. The angle of overlap χ can be used to evaluate the case. The χ is easily shown in a 2D drawing in Fig. 10 and usually stays in the range 30°–40° for clean water pump.

The blade of the impeller is shaped by adjusting the distributions of the velocity components from the leading edge to the trailing edge of the blade (Figs. 11 and 12). The distributions must be adjusted in order to find the best blade angle distribution or stacking condition on the blade exit. After plotting all the streamlines, it might be necessary to examine the surface sketch of the blade to avoid frequent undesirable

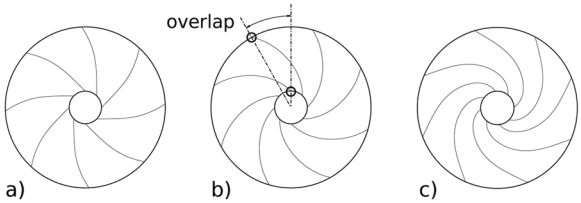

Fig. 10. Overlap qualitative representation.

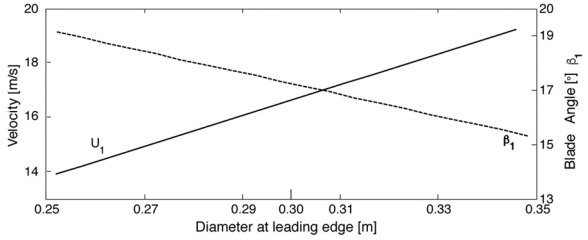

Fig. 11. Leading edge parameters of the blade profile.

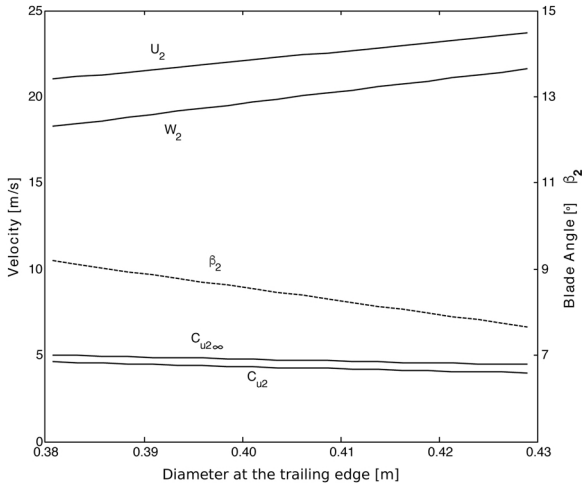

Fig. 12. Trailing edge parameters of the blade profile.

factors; the blade may be too long so that the overlap angle χ exceeds the maximum suggested and the inlet edge of the blade may deviate considerably from the correct radial direction. It is then necessary to make iterative corrections by shortening some streamlines and lengthening others and assuming the variation of the angle β_1 with a variation of the corresponding values of c_{m1} and the linked w_1. It is necessary to iterate the analysis and select the suitable blade thickness, curvature and vane swept angles – all extremely important from the manufacturing point of view.

5. CFD analysis

For the cost-effective design of any hydro-power project, it is therefore very important to predict the hydraulic behavior and efficiency of hydro turbines before they are used. An experimental approach would be much more costly and time consuming. Using CFD it is possible to gain significant insight into issues such as energy transfer and fluid flow details in hydraulic turbines [52–54] Only the final fine-tuning has to be done experimentally. This section presents the results of the first step of a CFD integrated design analysis for a Deriaz pump-turbine runner. The computations were carried out with the aid of the Numeca software FINE^{TM}/Turbo solver, with the additional assumption of stationary flow and using a second order discretization scheme. Carried out to double precision, the computations required around $3{\cdot}10^3$ iterations. Modifying the angle position of the runner blade involves adapting the mesh at blade-to-blade structure: closing the passage stretches the mesh, increasing skewness. In order to protect the mesh, different block definitions and more mesh points are used.

5.1. Solid prototype modeling

The Deriaz pump-turbine studied in this project was modeled with the CatiaV5 CAD tool. To model effectively it is important to avoid problems during the CFD analyses. Problems may occur during the grid generation phase if unwanted surfaces or solid parts remain from the solid modeling. The surfaces were drawn with the fewest features possible, using the original drawings in order to avoid any imperfections (e.g. sharp edges, open surfaces).

Computational domain and the runner profiles are shown in Fig. 13.

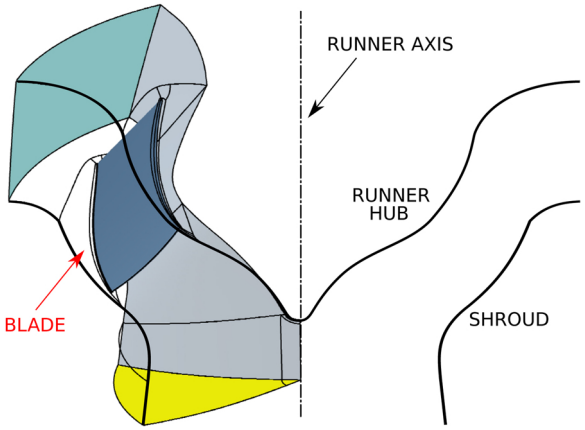

Fig. 13. Runner domain blocks and boundary condition surfaces.

5.2. Discretisation process

Generating the mesh is a critical step for turbomachine applications. Generally, over 50% of the time spent in industry on a CFD project is devoted to the definition of the domain geometry and grid generation [55]. Since a grid in these types of applications includes many technological effects (rotor tip clearance, hub leakage flow [56]), it might require over 2 million points for one blade passage. All available experience in CFD applications indicates that the mesh definition and quality has a considerable influence on accuracy and convergence properties. The boundary layer estimation is continuously corrected for the walls that define the geometry: the shroud, the hub, the blades and tip gaps between rotor and stator. Each surface has a different environment, and therefore needs to be treated differently. The velocity field is more complex in the gap rotor and stator than in the surrounding zones: the passage narrows abruptly and contains a rotating component. To asses the independence of the grid on the accuracy of the solution, a mesh convergence test is conducted (Table 6). It is considered sufficient to choose a mesh close to the stable solution of the hydraulic efficiency, η_h, of ± 0.05, that correspond to an initial mesh of the domain of about 3.1 million of nodes (Fig. 14). Care must be taken when evaluating the quality of mesh suitable to the selected turbulence model. A summary of the mesh characteristics is presented in Table 7. The discrete domain is composed by five blocks whose features change according to the operating conditions. A higher number of nodes are needed for the narrower blade to blade passage in order to maintain a minimum quality level.

Table 6
Mesh convergence test on the case at $\delta\beta = 5°$, $a = 56\%$ and mass flow of 0.18 [m^3/s].

	Nodes (million)	Min skewness	Efficiency, η_h	Torque, T [Nm]	CPU time [h]
Mesh 1	0.9	25	0.7858	234.2	3
Mesh 2	1.2	25	0.7872	228.0	4
Mesh 3	3.1	28	0.7956	230.5	11
Mesh 4	5.4	29	0.7980	230.8	16
Mesh 5	8.2	29	0.7976	231.9	27

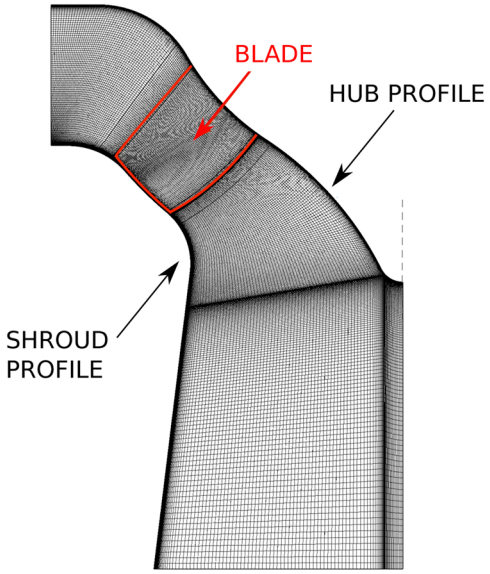

Fig. 14. Meridional view of the mesh.

Table 7
Mesh quality summary for turbine case at $\delta\beta = 5^{\circ}$ and closing runner blade at $\delta\beta = 0^{\circ}$.

Block	No. of nodes (million)	Minimum skewness	y^{+}_{max}	y^{+}_{min}
Case: $\delta\beta = 5^{\circ}$, $a_0 = 50\%$				
Pump bulb inlet	0.6	71	1.4	0.8
Blade topology	1.3	28	5.2	0.8
Tip radial clearance	0.7	28	6.0	3.6
Pump Outlet	0.5	86	1.6	0.6
Entire mesh	3.1	28	6.0	0.8
Case: $\delta\beta = 0^{\circ}$, $a_0 = 50\%$				
Pump bulb inlet	0.6	71	1.4	0.8
Blade topology	1.9	14	8.1	1.2
Tip radial clearance	0.9	15	12.1	3.5
Pump Outlet	0.5	86	1.6	0.9
Entire mesh	3.9	28	12.1	0.8

5.3. Numerical modeling of turbulent fluid flow

The grid size of the Deriaz runner comprises only one of 8 repetitions of the blade block. For selected cases, the accuracy of different meshes are examined in order to import a good mesh without using a large number of cells. The bigger the mesh, the more equations the software has to solve.

Simulations are computed with Coarse Grid Initialization that allows staring the iteration with a coarser level of the mesh and rapidly get closer to the possible finest level of the mesh until the convergence. The Courant-Friedrich-Levy number (CFL) has is given a constant value of 3 for the proposed setting according to FINE/Turbo. This number globally scales the time-step sizes used for the time-marching scheme of the flow solver. A higher CFL number results in a faster convergence, but will lead to divergence if the stability limit is exceeded [57].

Further attention in the hydraulic turbomachinery design must then be given to cavitation phenomena and the pressure distribution along the leading edge, trailing edge and the suction side of the blade adjusting the design each time as required. Cavitation occurs when in a liquid flow, the pressure falls below its saturation pressure, and as a consequence, gas/vapor bubbles are formed. Cavitation is, in many cases, an undesirable occurrence since it can produce structural damage as soon as the bubbles implode due to a increase of pressure. It can also cause instabilities, a loss in efficiency and an increase of the noise level. The effects of cavitation on the overall hydraulic efficiency is considered by mean a two-phase model dedicated to this phenomenon offered by the CFD software [57]. The model requests some parameters related to the fluid: the vapour pressure at the investigation temperature $P_v = 1227.89$ [Pa], density of the liquid phase $\rho_L = 999.7$ [kgm^{-3}], density of vapor phase $\rho_v = 9.38{\cdot}10^{-3}$ [kgm^{-3}]. It is also necessary define the slope of the barotropic state law

$$\rho = \frac{\rho_L + \rho_v}{2} + \frac{\rho_L - \rho_v}{2}\sin\left(\frac{P - P_v}{c^2_{\min}}\frac{2}{\rho_L - \rho_v}\right) \tag{27}$$

where c_{min} is the celerity of the sound in the homogeneous liquid–vapour mixture.

The convergence in these results is reached with CFL reduced at 0.8 Hence the simulation test results much slower and it needs a bigger number of iterations to reach the convergence and as predicted.

A mesh linked to a result of a hydraulic efficiency within a range of ± 0.05 is selected and it correspond to a mesh with around 3.1 million nodes initially. The time required to obtain results from the simulation is defined by the condition of convergence. It is therefore crucial to check for and assess convergence, and not only by examining residual levels. To gauge convergence properly, it is necessary to monitor other values: overall mass, momentum, energy and scalar balances are obtained. The net imbalance is recorded to be less than 0.3% of the net flux through the domain.

An analysis sequence in post-processing confirms the assumptions made during the design of the mixed-flow pump (Section 4). In Fig. 15, streamlines are shown coming from the inlet surface up to the leading edge of the pump blade; the flows appear orthogonal and uniform at the blade leading edge.

An appropriate turbulence model is chosen based on the specific application [56]. The choice of the turbulent model used is pragmatically based on the CPU-time required to reach convergence, even though the results obtained are within reasonable range of those given by the other solutions [58].

Close to the wall the flow is influenced by viscosity effects and does not depend on free stream parameters. The mean flow velocity depends on the distance from the wall, fluid density, fluid viscosity and the wall shear stress.

The selection of a suitable turbulence model is of paramount importance for the accuracy of the expected results. Choosing the wrong model may result in divergence from achievable results. This is particularly important when experimental verification is not feasible. Anyway, under such circumstances, the choice must be guided by operator experience, generated mesh parameters (appropriate y^{+}) and available CPU. To validate the range of the results of the simulations, another turbulent model test is carried out and summarized in Table 8.

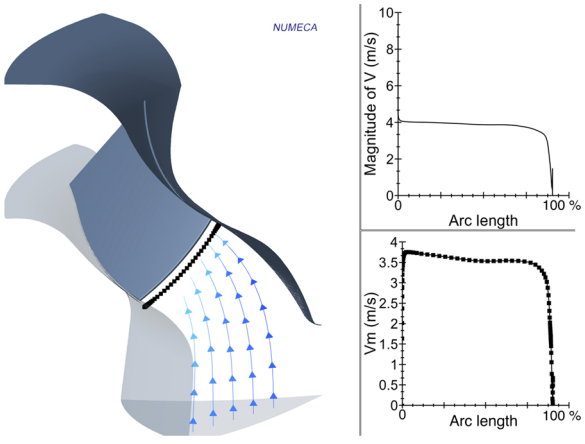

Fig. 15. Flow streamlines at the pump inlet.

Table 8
Turbulent model test for an assigned test and mesh of 3.1 nodes without cavitation model applied: Spalart-Allmaras (SA), SA with Extended Wall Function (EWF), k-ϵ models, k-ω, Shear Stress Transport (SST) and v2 code model (a seven equations model).

Model	$\Delta\dot{m}$ [%]	ΔP [kPa]	T [Nm]	η_h [%]	$\Delta\eta$ [%]	CPU-time [h]
SA	0.030	148.0	232.2	79.84	1.641	12.84
SA EWF	0.053	145.0	231.9	80.15	1.331	7.20
k-ϵ Yang Shih	0.123	145.1	232.0	80.64	0.841	18.67
k-ϵ EWF	0.197	143.0	235.0	81.26	0.221	18.56
k-ω	0.005	143.3	238.5	83.44	1.959	16.35
SST EWF	0.024	143.8	238.6	83.32	1.839	14.69
v2 code	0.312	145.9	239.3	81.63	0.149	23.17

5.4. Pump mode

Boundary conditions are fundamental to describing the test and imposing the correct equation sets to be solved. The pressures at the entrance and exit of the machine have to controlled and the velocity fields mapped, especially those which define the guide vanes' peculiarities in turbine mode. The behavior of the Deriaz type model was experimentally tested with a fixed static head of 10 m at the inlet under different angles of regulation of the guide vanes. The chosen rotational speed, N, is 1054 [rpm]. The boundary conditions are set to agree with the experimental data (Table 9). The pump mode testing simulations of the Deriaz machine aim to define the working points with the developed design. Its characteristic curves defined by positioning the angle of the runner blade at 0, +5, +10 and +15 degrees.

Due to the unknown flow distribution at the entrance of the machine, some adaptations are necessary. In order to facilitate the discharge, the mobile parts of the diffuser (the inlet guide vanes at in turbine mode) are kept fully open ($a_0 = a_{max} = 100\%$). This case was computed under the following settings: inlet pump total absolute pressure fixed at 201,000 Pa for all related patches and the velocity normal to the inlet of the domain. It is also necessary to consider some relationships for deriving the required turbulence quantities such as turbulent intensity, characteristic length and turbulent viscosity μ_t. The point of maximum efficiency of the machine in pump mode is slightly more than 0.82 and was recorded at maximum rotor blade aperture ($+10^\circ < \delta\beta < +15^\circ$) close at the design point of 0.24 m^3/s, $\delta\beta = +15^\circ$. Even more interesting is the possibility to maintain a higher efficiency of 0.79 for a wide range of flow rates: from about 0.12 to 0.28 m^3/s, the equivalent of $Q_D \pm 40\%$. Fig. 16 depicts the pump characteristic curves for the model of the Deriaz turbomachine with fully open turbine guide vanes at different blade angle position.

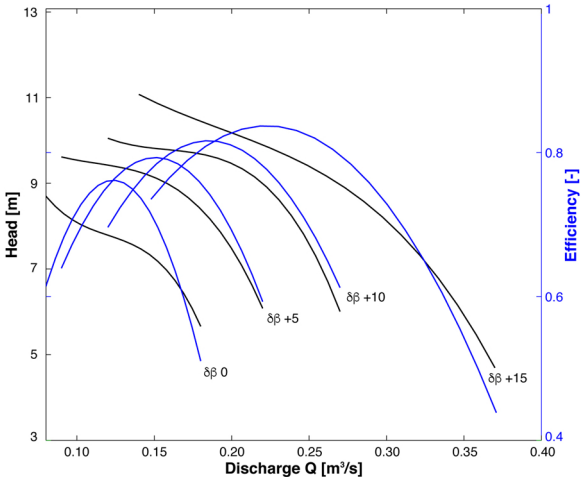

Fig. 16. Head and efficiency of Deriaz pump-turbine in pump mode at 0, +5, +10 and +15 blade angle position.

5.5. Turbine mode

During a complete design of the machine it is necessary to carry out several tests at the most important blade geometry and rotation speed, N, settings as well as for the guide vanes angles, β and Ω. The design process is iterative in that it tries to refine the design in the light of the results obtained at each design step. In generating mode tests the runner is rotating in the opposite direction than during pumping. This section illustrates two different cases of the machine in turbine mode.

The first case is with a variable blade pitch at fixed available head. Regulation is carried out by the adjustable blades of the runner blades. The inlet turbine (the outlet in pump mode), this time has a total absolute pressure fixed at 351 kPa with a variable flow direction to simulate the guide vanes. The turbine is submerged with an outlet static pressure of 201 kPa.

The designed downsized Deriaz pump turbine provides a good picture of the performance in turbine mode. In order to provide a qualitative comparison with the experimental data, an important overview of the efficiency curve is shown from manufacturer report tests in [34–36] and represented by Fig. 17. Mechanical losses, not implemented in the CFD simulation, appear to be the main cause of small discrepancy in the efficiency peaks.

In the second case the impeller has fixed geometry and runs with variable guide vanes opening. In this test, the chosen pitch angle of the rotor blades is selected to +5 degrees. The simulations have the following inlet conditions: mass flow and flow directions (Table 10). The

Table 9
Boundary conditions summary used in the CFD simulations.

	Pump mode	Turbine mode	Turbine mode: Case 2
Inlet	Total pressure at 201,000 Pa Velocity normal to the surface Turbulent intensity of 8%	Total pressure at 351,000 Pa Variable flow direction	Mass flow Variable flow direction
Outlet	Mass flow	Total pressure at 201,000 Pa	Total pressure at 201,000 Pa
Solid	Rotating at 1054 rpm Rough wall type	Rotating at −952 rpm Rough wall type	Rotating at −952 rpm Rough wall type
Blade angle	$0^\circ < \delta\beta < +15^\circ$	$0^\circ < \delta\beta < +15^\circ$	$\delta\beta = +5^\circ$
Guide vane	Fully open	$17\% < a_0 < 100\,\%$	$17\% < a_0 < 100\,\%$

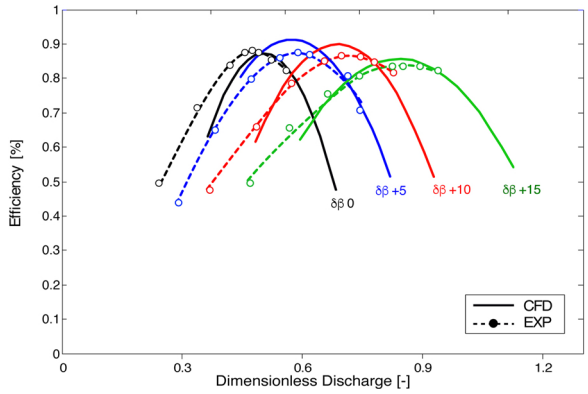

Fig. 17. Measured and numerical performance in turbine mode at variable runner blade angle at fixed vanes versus dimensionless discharge Q/Q_{11}.

outlet draft tube has the averaged static pressure set at 201 kPa with back flow control. In this case study, the selected turbine Deriaz has a fixed runner blade angle of $\delta\beta$ +5° and fixed rotation speed. The different open gate vane values, a_0/a_{max} [%], admit a controlled mass flow rate and allow the required ΔP to change. All the possible combinations of settings are thus mapped.

The flow direction at the entrance is defined by the angle α ranging from 0° to 43° respectively at closed and fully open guide vanes. The throat passage at the vanes changes from 0 mm to 36 mm, affecting flow rate and direction (Table 10). Fig. 18 shows how an excessive opening of the flow affects the orientation of the current which then fails to apply a torque to the rotor blades. This lowers efficiency and also it does not succeed in disposing a higher flow rate than was theoretically expected.

For a turbine at limited available head, H, the peak of hydraulic efficiency (91%) coincides with the combination of a rotor blade closer to level $\delta\beta = +5°$ and an inlet direction flow generated by 25% of the maximum granted by the guide vanes: such direction helps achieve an effective angular momentum in the energy balance to the turbine. Forces and torque are calculated from the pressure and velocity fields on the walls, including rotating solid boundary characteristics (Fig. 19). Furthermore, although the mapping efficiency was realized exclusively in the case of a turbine at $\delta\beta = +5°$ at different flow orientations, it does illustrate the full versatility over a large area of high efficiency (Fig. 20).

According to the IEC standard nomenclature [37], Thoma number, σ, is the dimensionless term indicating the conditions of cavitation under which the machine operates. It is expressed as the ratio of Net Positive Suction specific Energy NPSE to a specific hydraulic energy $E = gH_1 - gH_2$.

$$\sigma = \frac{\text{NPSE}}{E} \simeq \frac{\frac{P_a - P_v}{\rho} - \text{gh}_s}{E} \tag{28}$$

where h_s is the machine setting level. Clearly every flow has a value of σ whether or not cavitation occurs. The cavitating performance, as illustrated in Fig. 21 for $\delta\beta = +5°$, is presented as a family of curves for a given flow condition by the guide vane opening (at 33%, 50% and 100%). Besides the hydraulic efficiency, η_h, other factors are

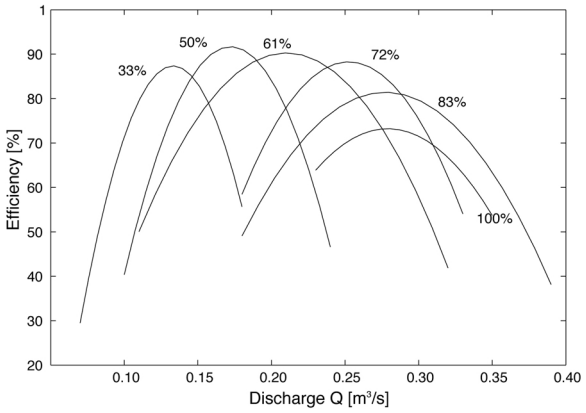

Fig. 18. Efficiency map of Deriaz turbine at $\delta\beta$ + 5 blade angle and variable guide vane direction: opening from 33% up to 100%.

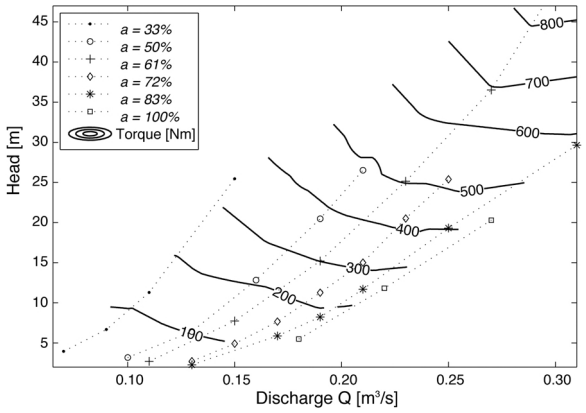

Fig. 19. Torque map of Deriaz turbine at fixed runner blade angle $\delta\beta$ + 5 and variable guide vane opening from 33% up to 100%.

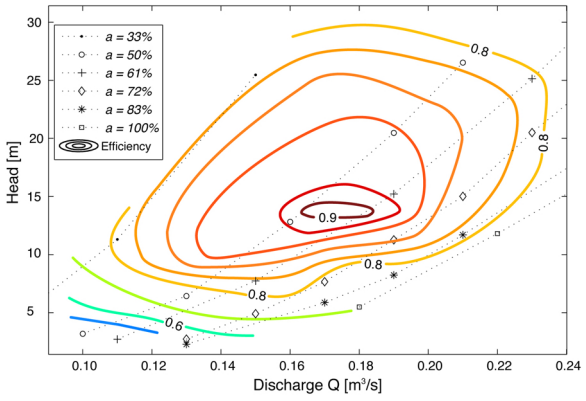

Fig. 20. Hill chart of Deriaz turbine at fixed runner blade angle $\delta\beta$ + 5 and variable guide vane direction.

Table 10
Inlet condition for the flow direction in turbine mode.

Throat vane [mm]	6	8	12	18	22	26	30	36
Opening a_0 [%]	17	22	33	50	61	72	83	100
c_r/c	−0.1136	−0.1516	−0.2273	−0.3410	−0.4226	−0.5000	−0.5683	−0.6820
c_u/c	−0.9935	−0.9884	−0.9738	−0.9401	−0.9063	−0.8660	−0.8228	−0.7314

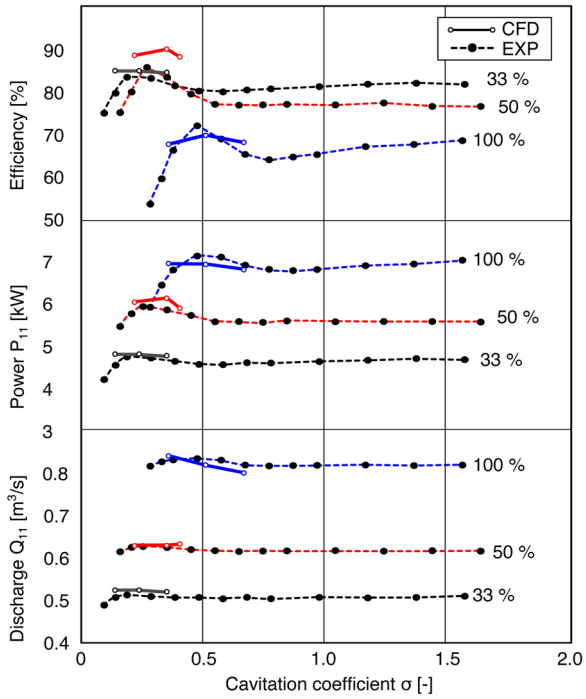

Fig. 21. Cavitation curve for the model Deriaz turbine at $\delta\beta = +5°, -952$ rpm and for a given guide vane opening angle.

represented

$$P_{11} = \frac{P}{D^2H^{1,5}} \quad Q_{11} = \frac{Q}{D^2H^{0,5}} \tag{29}$$

While σ decreases, observations of the cavitation onset and the cavity development are reported. The peak of efficiency matches with the opening at 50%. The influence of the cavitation development on the turbine efficiency is observed more relevant for high discharge or high load (100% opening).

6. Deriaz pump-turbine outlooks and opportunities

Worldwide PHES is the most established and common storage technology and the use of Deriaz pump-turbines provides a valid solution due to their high hydraulic efficiency and adaptability. In order to produce a pump-turbine, a pump impeller usually gives the designing starting point. Indeed, common turbines have usually lower performance in pump mode. For instance, the blades relatively short of a Francis turbine runner lead to an excessive slowing down of the waterflow in pump mode, producing flow detachment and efficiency loss. Moreover, the Francis turbine blade's angle is too large to produce a stable characteristic in pump mode. The concept of pump-turbine as a trade-off between pump impeller and turbine runner is required. Besides, the optimal functioning point of the common hydraulic turbomachine in turbine mode does not match with its operation in pump mode. At constant speed, the best efficiency point in turbine mode corresponds to a higher head than for the pump mode. Moreover, the divergence between the operating points is enhanced because turbines work below the static head (reduced by hydraulic losses) and the delivered head by pumps is greter than the net head. The design of Deriaz pump-turbine with double regulation by guide vanes and runner blades solves the discrepancy between pumping and generating modes. In this way pressure pulsations and cavitation can be avoided over the total range of variation in flow and head. Compared to the Kaplan turbines, Deriaz prototypes use a diagonal flow direction to enlighten the hydraulic load and can be applied under higher head, competing with Francis turbines. For low head Francis turbines, part-load operation at higher head than the design head is a general problem [59] which can be avoided by using adjustable blade turbines. Within this frame, Deriaz pump-turbine fills the gap left by the reversible Francis and Kaplan turbines.

In addition to their improved efficiency over a wide load range as a result of runner blade adjustments, Deriaz turbomachines can also work under variable rotation speeds. Some PHES systems couple the motor/generator to a frequency changer enabling a wider range of pumping or generating speeds (± 12%) [60]. Although a Francis turbine can also benefit from this technology, it has been shown that a variable speed Deriaz can take about 1.5 times the input capacity of a Francis turbine with variable frequency driver [61].

It is now clear that the extra degree of freedom present in a Deriaz pump-turbine allows a variable power produced and consumed better than other hydraulic pump-turbines in function of the needs of the grid. Thus, Deriaz in PHES applications is a very attractive solution for Balance Responsible Parties (BRP) in grid balancing. Nowadays, BRPs have to deal with the growing share of intermittent renewable energy sources who has led to increased interest in flexibility and storage capacity [62]. By 1960, when most of the Deriaz turbomachines have been installed (Table 1), the energy mix has been diversifying significantly: the world had moved into nuclear electricity production and today's renewables (modern biofuels, wind, and solar) appeared only in the 1980–1990s in the global total energy production. Compared to the applications of the 1960s, nowadays the regulation systems as the one applied to the adjustable runner blades are not more expensive, but more advanced materials and solutions are used to improve operational and power characteristics. Since then, the economics, the needs and the energy market have been also changed and new opportunities exploration and reassessing previous technologies are indispensable to achieve the recent energy targets. Multiple storage solutions must now be analysed at all scales and for various exploitable working conditions. Fluctuations in the renewable energy surplus necessitate the technology to manage energy storage efficiently and to help meet electric grid requirements providing critical capacity during key energy need periods. Deriaz performance and its higher cavitation resistance at part-load lead to high flexibility and allow the increase of the exploitable hydropower site and revenues in PHES applications.

7. Conclusions

Deriaz pump-turbines have never been reviewed and modelled in the literature nor discussed for a downsized model for micro-PHES applications which is extremely suited to our current energy generation and storage needs. This paper describes the Deriaz pump-turbine and all the preliminary steps of its design. The robust and accessible hydraulic modeling, here presented, favors designs capable of operating at high efficiencies over wider operating ranges. The analysis is conducted on a downsized model of Deriaz pump-turbine for micro PHES applications and it evaluates its potential, providing a guide to its design, scaling, and adaptation to pumped hydro. Design runner, CFD and experimental results are found to be in agreement regarding the characteristic curves and performance. Although a further refinement of the model design might give a slightly better hydraulic performance, this paper provides a practical and easily-built method to implement a Deriaz pump-turbine solution which gives a good outline at its first iteration. In pump mode, a minimum of hydraulic efficiency of 80% is registered for a wide range of discharge load $Q_D \pm 40$ %. In turbine mode, the peak of hydraulic efficiency is modelled at 91% with opening guide vanes. As expected, the combined use of a variable blade pitch with moving guide vanes provides a wider range of highly efficient working conditions making a Deriaz pump-turbine a very suitable turbomachine solution at high-variable load. The results show clearly how the downsizing of the prototype can conserve versatility over a wide range of partial load. According to the data collected and produced in this paper, the application ranges of the micro-size of Deriaz turbine can be now compared

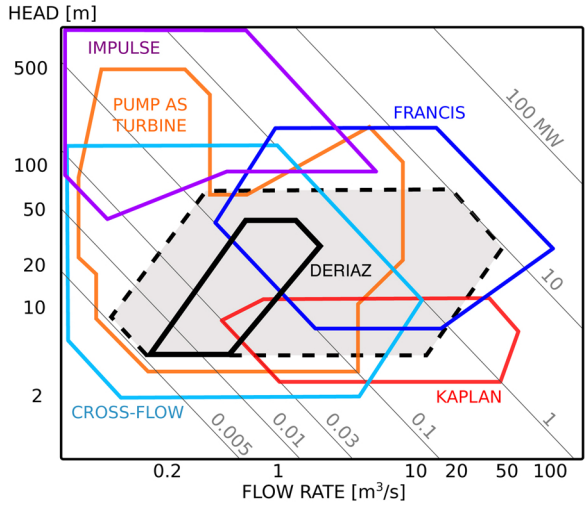

Fig. 22. Types of hydraulic turbines and Deriaz turbine in their application area Q-H for micro-hydropower. Adapted from [7,63–65] and authors' data.

to the other hydraulic turbines and be plotted in solid black line in Fig. 22. The shaded region marked in dashed line shows the predicted extension of Deriaz application range thanks adjusted angle blades and different runner sizes.

We conclude that the computational analysis method and the design parameters employed in this study can be effectively applied to the hydraulic design and optimization process of a Deriaz mixed-flow pump-turbine runner. The analysis on the pump-turbine type Deriaz enhances the discussion of PHES and micro-PHES and their new unexplored opportunities.

Acknowledgements

This research was supported by the Walloon Region in the framework of the SmartWater project. Authors wish to acknowledge the DG04, DG06 and Service Public de Wallonie for their continuous support.

References

[1] O. Palizban,, K. Kauhaniemi, Energy storage systems in modern grids? Matrix of technologies and applications, J. Energy Storage (2016), https://doi.org/10.1016/j.est.2016.02.001.
[2] L. Barelli, G. Bidini, F. Bonucci, A. Ottaviano, Residential micro-grid load management through artificial neural networks, J. Energy Storage (2018), https://doi.org/10.1016/j.est.2018.03.011.
[3] K.S. Balkhair, K.U. Rahman, Sustainable and economical small-scale and low-head hydropower generation: a promising alternative potential solution for energy generation at local and regional scale, Appl. Energy 188 (Supplement C) (2017) 378–391, https://doi.org/10.1016/j.apenergy.2016.12.012.
[4] I. Yüksel, Hydropower for sustainable water and energy development, Renew. Sustain. Energy Rev. 14 (1) (2010) 462–469, https://doi.org/10.1016/j.rser.2009.07.025.
[5] K.D. Strang, Feasibility of a hidden renewable energy hydro power storage battery, J. Energy Storage (2017), https://doi.org/10.1016/j.est.2017.07.001.
[6] C.J. Blanco, Y. Secretan, A.L. Mesquita, Decision support system for micro-hydro power plants in the Amazon region under a sustainable development perspective, Energy Sustain. Dev. (2008), https://doi.org/10.1016/S0973-0826(08)60435-4.
[7] A. Morabito, P. Hendrick, Pump as turbine applied to micro energy storage and smart water grids: a case study, Appl. Energy 241 (2019) 567–579, https://doi.org/10.1016/j.apenergy.2019.03.018.
[8] S.P. Koko, K. Kusakana, H.J. Vermaak, Optimal power dispatch of a grid-interactive micro-hydrokinetic-pumped hydro storage system, J. Energy Storage (2018), https://doi.org/10.1016/j.est.2018.02.013.
[9] P.P. Jonsson, B.G. Mulu, M.J. Cervantes, Experimental investigation of a Kaplan draft tube – Part II: Off-design conditions, Appl. Energy 94 (2012) 71–83, https://doi.org/10.1016/j.apenergy.2012.01.032.
[10] P. Deriaz, La turbine-pompe réversible axio-centrifuge à pas variable: le développement d'une nouvelle machine hydraulique, Bull. Tech. Suisse Romande Ecole polytechnique federale Zurich: centenaire 1855–1955 (December (2)) (1955) 382–387, https://doi.org/10.5169/seals-61375.
[11] G. de Oliveira e Silva, P. Hendrick, Pumped hydro energy storage in buildings, Appl. Energy 179 (2016) 1242–1250, https://doi.org/10.1016/j.apenergy.2016.07.046.
[12] S. Few, O. Schmidt, A. Gambhir, Energy access through electricity storage: insights from technology providers and market enablers, Energy Sustain. Dev. (2019), https://doi.org/10.1016/j.esd.2018.09.008.
[13] A. Morabito, J. Steimes, O. Bontems, G. Al Zohbi, P. Hendrick, Set-up of a pump as turbine use in micro-pumped hydro energy storage: a case of study in Froyennes Belgium, J. Phys. Conf. Ser. 813 (2017), https://doi.org/10.1088/1742-6596/813/1/012033.
[14] P. Deriaz, "Hydraulic turbine," Dec. 21 1926. US Patent 1611341.
[15] A. Skotak, P. Stegner, Choosing turbines for low-head pumped-storage plants, HRW-Hydro Rev. Worldw. 22 (January) (2014).
[16] P. Deriaz, J. Warnock, Reversible pump turbine for Sir Adam Beck-Niagara pumping-generating station, Trans. ASME 81 (December) (1959) 521–533.
[17] M. Johnson, P. O'Connor, R. Uria-Martinez, 2017 Hydropower Market Report – Update (April), Tech. Rep. Oak Ridge National Laboratory, 2018.
[18] A.S. Lopes, R. Castro, C. Silva, Metaheuristic methods applied to the pumps and turbines configuration design of water pumped storage systems, J. Energy Storage (2018), https://doi.org/10.1016/j.est.2018.05.006.
[19] T. Maricic, D. Haber, S. Pejovic, Niagara pump generating station proven functionality unique in canada, Electrical Power & Energy Conference (EPEC), 2009, IEEE, 2009, pp. 1–6 IEEE.
[20] C.M. Roberts, E.B. Wilson, J.G. Wiltshire, Design aspects of the strathfarrar and kilmorack hydroelectric scheme, Proc. Inst. Civil Eng. 30 (3) (1965) 449–487, https://doi.org/10.1680/iicep.1965.9522.
[21] A. Erskine, O. Van Rooy, The complete refurbishment of Culligran underground hydropower station, Hydropower Developments – New Projects, Rehabilitation, and Power Recovery, vol. 2004 6 (2004) 125–140.
[22] A. Imanishi, Fuji Hydraulic Turbine and Generator II vol. 10(6, (1964).
[23] S. Zhang, P. Andrews-Speed, P. Perera, The evolving policy regime for pumped storage hydroelectricity in China: a key support for low-carbon energy, Appl. Energy 150 (Supplement C) (2015) 15–24, https://doi.org/10.1016/j.apenergy.2015.03.103.
[24] M. Castillo, El aprovechamiento hidroeléctrico del tajo inferior y las centrales des bombeo, Revista de obras publicas, 1964.
[25] J. Houdeline, J. Verzeroli, Deriaz pump-turbine for Naussac 2 plant in France, ALSTOM Power Hydro, 1999.
[26] O. Thapar, Modern Hydroelectric Engineering Practice in India: Electro-Mechanical Works, (2017) . [Visited online: 30 November] http://ahec.org.in/publ/Modern_Hydroelectric_Engineering_Practice_Prof_OD_Thapar/Volume_I/Chapter-3_Hydraulic_Turbine_Classification_and_Selection.pdf.
[27] C.K.D. Blansko Engineering, New Hydropower Projects Under Construction in India, (2012) [Visisted online: 30 November 2017].
[28] Individual Individual Units for Hydro in Japan, http://globalenergyobservatory.org. [Visited online: 30.11.17.
[29] http://www.zzw-niedzica.com.pl/elektrownia.htm. [Visited online: 30.11.17].
[30] C.K.D. Blansko Engineering, Company's Reference Project, (2012) [Visited online: 30 November 2017] http://www.ckdlh.cz/en/about-us/companys-reference-projects.
[31] Slovenske Elektrarne, https://www.seas.sk/liptovska-mara-hpp. [Visited online: 30.11.17].
[32] F.O. Ruud, Vibration of deriaz pumps at Dos Amigos pumping plant, J. Fluids Eng. 98 (8) (1976) 674–679, https://doi.org/10.1115/1.3448447.
[33] J.J. Kirejczyk, J. Verzeroli, Non-Polluting Pump Turbine: Naussac 2, (2001) Hydrovision 2000, Charlotte - USA, alstom power hydro ed..
[34] M. Zavadil, M. Meduna, Essais sur le modele reduit, Hampton, Virginia: GEC. ALSTOM Neyrpic, 1981.
[35] M. Zavadil, M. Meduna, Performances en Turbine, GEC, ALSTOM Neyrpic, Hampton, Virginia, 1981.
[36] M. Zavadil, M. Meduna, Performances en Turbine Model Test, GEC. ALSTOM Neyrpic, Hampton, Virginia, 1981.
[37] IEC, Hydraulic Turbines, Storage Pumps and Pump- Turbines-Model Acceptance Tests, IEC 60193 Standard – International Electrotechnical Commission Geneva, 1999, p. 578.
[38] R. Capata, E. Sciubba, Experimental fitting of the re-scaled Balje maps for low-reynolds radial turbomachinery, Energies 8 (8) (2015) 7986–8000, https://doi.org/10.3390/en8087986.
[39] J.F. Gulich, Centrifugal Pumps, 2nd ed., Springer, 2010.
[40] C. Pfleiderer, Turbomachines, Springer-Verlag, 1952.
[41] H. Davis, H. Kottas, A. Moody, The influence of reynolds number on the performance of turbomachinery, Trans. ASME 73 (July) (1951).
[42] A. Lipej, C. Poloni, Design of Kaplan runner using multiobjective genetic algorithm optimization, J. Hydraul. Res. 38 (1) (2000) 73–79, https://doi.org/10.1080/00221680009498361.
[43] S. Muntean, I. Draghici, G. Gînga, L.E. Anton, A. Baya, Hydrodynamic design of a storage pump impeller using inverse method and experimental investigation of the global performances, WasserWirtschaft Extra 1 (2015) 28–32.
[44] G. Peng, S. Cao, M. Ishizuka, S. Hayama, Design optimization of axial flow hydraulic turbine runner: Part I – An improved Q3D inverse method, Int. J. Numer. Methods Fluids 39 (6) (2002) 517–531, https://doi.org/10.1002/fld.342.
[45] G. Peng, S. Cao, M. Ishizuka, S. Hayama, Design optimization of axial flow hydraulic turbine runner: Part II – Multi-objective constrained optimization method, Int. J. Numer. Methods Fluids 39 (6) (2002) 533–548, https://doi.org/10.1002/fld.343.
[46] R. Susan-Resiga, S. Muntean, F. Avellan, I. Anton, Mathematical modelling of swirling flow in hydraulic turbines for the full operating range, Appl. Math. Model.

35 (10) (2011) 4759–4773, https://doi.org/10.1016/j.apm.2011.03.052.
[47] S. Lazarkiewicz, A.T. Troskolanski, Impeller Pumps, Pergamon Press, 1965.
[48] A.J. Stepanoff, Centrifugal and Axial Flow Pumps, Design and Applications, 1st ed., John Wiley and Sons Inc, 1957.
[49] L. Tan, B. Zhu, S. Cao, Y. Wang, B. Wang, Influence of prewhirl regulation by inlet guide vanes on cavitation performance of a centrifugal pump, Energies 7 (2) (2014) 1050–1065, https://doi.org/10.3390/en7021050.
[50] F. Wiesner, A review of slip factors for centrifugal impellers, J. Eng. Power 89 (4) (1967) 558–566.
[51] T.W. von Backström, A unified correlation for slip factor in centrifugal impellers, J. Turbomach. (2005).
[52] H.J. Choi, M.A. Zullah, H.W. Roh, P.S. Ha, S.Y. Oh, Y.H. Lee, CFD validation of performance improvement of a 500 kW Francis turbine, Renew. Energy 54 (2013) 111–123, https://doi.org/10.1016/j.renene.2012.08.049.
[53] Y. Wu, S. Liu, H.S. Dou, S. Wu, T. Chen, Numerical prediction and similarity study of pressure fluctuation in a prototype Kaplan turbine and the model turbine, Comput. Fluids (2012), https://doi.org/10.1016/j.compfluid.2011.12.005.
[54] A.V. Minakov, D.V. Platonov, A.A. Dekterev, A.V. Sentyabov, A.V. Zakharov, The numerical simulation of low frequency pressure pulsations in the high-head Francis turbine, Comput. Fluids (2015), https://doi.org/10.1016/j.compfluid.2015.01.007.
[55] H.K. Versteeg, W. Malalasekera, An Introduction to Computational Fluid Dynamics: The Finite Volume Method, Pearson Education, 2007.
[56] L.Y. Gicquel, N. Gourdain, J.-F. Boussuge, H. Deniau, G. Staffelbach, P. Wolf, T. Poinsot, High performance parallel computing of flows in complex geometries, C. R. Méc. 339 (2-3) (2011) 104–124, https://doi.org/10.1016/j.crme.2010.11.006.
[57] International NUMECA, User Manual FINE/Turbo 90.3, (2013).
[58] S.R. Shah, S.V. Jain, R.N. Patel, V.J. Lakhera, CFD for centrifugal pumps: a review of the state-of-the-art, Proc. Eng. (2013), https://doi.org/10.1016/j.proeng.2013.01.102.
[59] R.K. Turton, Principles of Turbomachinery, Springer Science & Business Media, 2012.
[60] H. Schlunegger, A. Thöni, 100 MW full-size converter in the Grimsel 2 pumped-storage plant, Proc. 2013 HYDRO Conference (2013).
[61] K. Miyagawa, N. Fukuda, K. Tsuji, K. Suzuki, J. Saotome, Development of a deriaz type pump-turbine with high head, large capacity and variable speed, Proceedings of the XIX IAHR symposium on hydraulic machinery and cavitation (1998) 39.
[62] A.S.M. Khan, R.A. Verzijlbergh, O.C. Sakinci, L.J. De Vries, How do demand response and electrical energy storage affect (the need for) a capacity market? Appl. Energy 214 (2018) 39–62, https://doi.org/10.1016/j.apenergy.2018.01.057.
[63] ANDRITZ, (2019) https://www.andritz.com/products-en/hydro/markets/small-mini-hydropower-plants.
[64] SULZER, (2019) https://www.sulzer.com/en/shared/applications/2017/05/29/09/07/hydraulic-power-recovery-turbine.
[65] O. Paish, Micro-hydropower: status and prospects, Proc. Inst. Mech. Eng. Part A: J. Power Energy 216 (1) (2002) 31–40, https://doi.org/10.1243/095765002760024827.